




Anticoncentration and magic spreading under ergodic quantum dynamics

Emanuele Tirrito ^{1,2}, Xhek Turkeshi ³, and Piotr Sierant ⁴

¹The Abdus Salam International Centre for Theoretical Physics (ICTP), Strada Costiera 11, 34151 Trieste, Italy

²Dipartimento di Fisica “E. Pancini”, Università di Napoli “Federico II”, Monte S. Angelo, 80126 Napoli, Italy

³Institut für Theoretische Physik, Universität zu Köln, Zùlpicher Strasse 77, 50937 Köln, Germany

⁴Barcelona Supercomputing Center, Barcelona 08034, Spain

(Dated: December 16, 2024)

Quantum state complexity metrics, such as anticoncentration and magic, offer key insights into many-body physics, information scrambling, and quantum computing. Anticoncentration and equilibration of magic under dynamics of random quantum circuits occur at times scaling logarithmically with system size, a prediction that is believed to extend to more general ergodic dynamics. This work challenges this idea by examining the anticoncentration and magic spreading in one-dimensional ergodic Floquet models and Hamiltonian systems. Using participation and stabilizer entropies to probe these resources, we reveal significant differences between the two settings. Floquet systems align with random circuit predictions, exhibiting anticoncentration and saturation of magic at time scales that increase logarithmically with system size. In contrast, Hamiltonian dynamics deviate from the random circuit predictions and require times scaling approximately linearly with system size to achieve saturation of participation and stabilizer entropies, which remain smaller than that of the typical quantum states even in the long-time limit. Our findings establish the phenomenology of participation and entropy growth in ergodic many-body systems and emphasize the role of energy conservation in constraining anticoncentration and magic dynamics.

Introduction. Understanding the propagation of quantum complexity metrics, such as entanglement [1, 2], anticoncentration [3], and magic resources [4], offers foundational insights into conceptual challenges of many-body physics, including quantum chaos, information scrambling and the emergence of statistical mechanics [5–9]. Addressing these problems for specific systems is notoriously difficult, as it requires unraveling the intricate structure of many-body states and computing non-linear measures such as entanglement [10], participation [11–13], and stabilizer entropies [14–16]. In this context, random quantum circuits have emerged as a powerful and analytically tractable framework for exploring quantum dynamics [17–20], bridging conceptual insights from many-body physics [21–25, 27] to applications in quantum computing [28–30]. A cornerstone result has been understanding the propagation of entanglement [31], elegantly captured by the membrane picture [32–37].

More recently, random quantum circuits allowed to resolve the evolution of anticoncentration and magic state resources. Anticoncentration, or Hilbert space delocalization, quantifies how much a state spreads in the computational basis [3, 38]. Magic resources, or nonstabilizer-ness [39–41], measure how much a state deviates from being a stabilizer state [42, 43]. Within random quantum circuits, these properties exhibit similar phenomenology, reaching the stationary value of typical many-body states in a timescale that is logarithmic in the system size $t_{\text{sat}} \propto \log_2(N)$ [3, 44–49]. Significantly, the rapid anticoncentration and magic spreading differs from the ballistic increase of the entanglement entropy, whose saturation timescale is linear in the system size $t_{\text{sat}} \propto N$.

Since their introduction, the success of random quantum circuits is tied with arguments of typicality, lead-

ing to the widespread belief that they capture the qualitative features of nearly all ergodic quantum systems. This work challenges that assumption by examining the dynamics of ergodic Floquet [50] and Hamiltonian systems [51]. Our findings uncover significant qualitative differences: while Floquet systems largely align with predictions from random circuit models, Hamiltonian systems exhibit markedly distinct dynamical behaviors within accessible system sizes. We attribute these discrepancies to the intrinsic structure of Hamiltonian systems, particularly the constraints imposed by energy conservation. These constraints strongly affect the intrinsic basis dependence of anticoncentration and magic measures, resulting in deviations from the universal behavior predicted by random circuits. In particular, we find that in Floquet dynamics, the participation entropy and the stabilizer entropy saturate, within fixed tolerance $\varepsilon < 1$, to the Haar stationary values in a timescale $t_{\text{sat}} \propto \log_2(N)$. Instead in the case of Hamiltonian dynamics with energy conservation, we observe a longer saturation time $t_{\text{sat}} \propto N$, both for the participation and stabilizer entropy, see Fig. 1.

Quantities of interest. We study a quantum chain of N qubits, with total Hilbert space dimension $D = 2^N$.

We will estimate anticoncentration with the participation entropy (PE), which quantifies the spreading of a state over a basis \mathcal{B} . For a many-body state $|\Psi\rangle$ the PE in the computational basis $\mathcal{B}_N = \{|\mathbf{x}\rangle\}_{\mathbf{x}=0}^{D-1}$ is

$$\mathcal{S}_k(|\Psi\rangle) = \frac{1}{1-k} \log_2 \left[\sum_{\mathbf{x} \in \mathcal{B}_N} p_{\mathbf{x}}^k \right], \quad p_{\mathbf{x}} \equiv |\langle \mathbf{x} | \Psi \rangle|^2, \quad (1)$$

where $p_{\mathbf{x}}$ is the probability to find the system in basis state $|\mathbf{x}\rangle$. Notice that \mathcal{S}_1 is defined by taking the limit

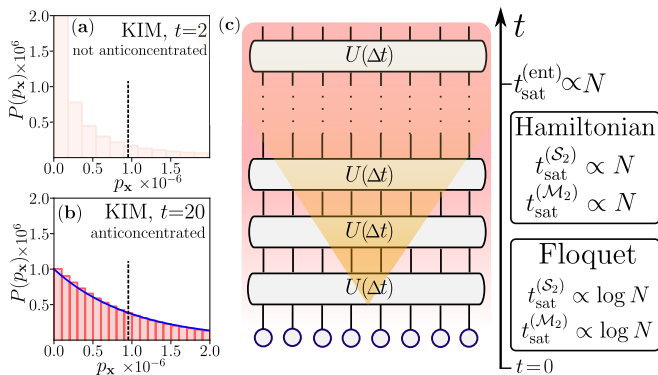


Figure 1. Anticoncentration and magic resources under the dynamics of many-body system with time-evolution operator $U(\Delta t)$. The distribution of probabilities $p_{\mathbf{x}}$ changes from being concentrated at small evolution time t , (a), to being anticoncentrated at large t , (b), and following the Porter-Thomas distribution [52, 53] (blue line). (c) Entanglement, PE, \mathcal{S}_2 , and magic resources (quantified by SE, \mathcal{M}_2) increase and reach, up to a fixed accuracy ϵ their saturation values at times $t_{\text{sat}}^{(\text{ent})}$, $t_{\text{sat}}^{(\mathcal{S}_2)}$, $t_{\text{sat}}^{(\mathcal{M}_2)}$.

$k \rightarrow 1$ in (1) and that $\mathcal{S}_k \geq 0$, with equality holding if and only if $|\Psi\rangle$ is a state of the computational basis. In general, the system size dependence of the PE is [54–56]

$$\mathcal{S}_k(|\Psi\rangle) = D_k N + c_k, \quad (2)$$

where D_k is the multifractal dimension and c_k is the subleading term [12, 13, 57]. For $D_k = 0$, the state $|\Psi\rangle$ is completely localized, while for $D_k = 1$ the state is fully extended. In the intermediate case, $0 < D_k < 1$, when D_k depends non trivially on the index k the state is said to be multifractal. The PE \mathcal{S}_2 is proportional to the logarithm of collision probability $p_{\text{col}} = \sum_{\mathbf{x} \in \mathcal{B}_N} p_{\mathbf{x}}^2$. The anticoncentration of state $|\Psi\rangle$ in basis \mathcal{B}_N , required by arguments of classical hardness of the sampling problems [58–61], occurs [3] when $p_{\text{col}} \leq a^{-1}2^{-N}$, where $0 \leq a \leq 1$ is a constant. In terms of the PE scaling (2), the anticoncentration requires $D_k = 1$ and $c_k \leq 0$ and can be verified on the level of the distribution of $p_{\mathbf{x}}$, see Fig. 1 (a), (b).

We quantify magic via the stabilizer entropy (SE), defined for a state $|\Psi\rangle$ in terms of the Pauli strings on N qubits $\mathcal{P}_N \equiv \{P_1 \otimes P_2 \otimes \dots \otimes P_N\}_{\{P_j=I,X,Y,Z\}}$ as [14]

$$\mathcal{M}_k(|\Psi\rangle) = \frac{1}{1-k} \log_2 \left[\sum_{P \in \mathcal{P}_N} D^{k-1} \Xi_P^k \right], \quad \Xi_P = \frac{\langle \Psi | P | \Psi \rangle^2}{D}, \quad (3)$$

with Ξ_P the Pauli spectrum [62, 63]. Again, \mathcal{M}_1 is defined by the limit $k \rightarrow 1$ in (3), and $\mathcal{M}_k \geq 0$, with the equality holding if and only if $|\Psi\rangle$ is a stabilizer state [64, 65]. A figure of merit of Eq. (3) is its efficient computability for matrix product states [16, 66–70].

Eqs. (1) and (3) highlight a similarity between anticoncentration and magic spreading when \mathcal{P}_N is viewed as a basis in the operator space. In particular, both

PE and SE are basis dependent quantities. Several connections between PE and SE have been found in recent works [16, 48, 70–72].

Methods and models. Our main goal is to understand the growth of PE and SE under the dynamics of ergodic quantum many-body systems and, in particular, to determine the timescales at which PE and SE saturate to their long-time stationary values. We define $\Delta \mathcal{S}_k(t) = \mathcal{S}_k^\infty - \mathcal{S}_k(t)$, representing the deviation of the time-evolving participation entropy $\mathcal{S}_k(t)$ from the long-time saturation value $\mathcal{S}_k^\infty \equiv \lim_{t \rightarrow \infty} \mathcal{S}_k(t)$, as a measure of the Hilbert space delocalization. Similarly, we define $\Delta \mathcal{M}_k(t) = \mathcal{M}_k^\infty - \mathcal{M}_k(t)$ as the deviation of the time-evolving stabilizer entropy from its stationary value $\mathcal{M}_k^\infty \equiv \lim_{t \rightarrow \infty} \mathcal{M}_k(t)$, serving as a measure for magic spreading. For local random one-dimensional unitary circuits of sufficient depth t , it is established [3, 45, 48] that

$$\Delta \mathcal{S}_k(t) = A_s e^{-\alpha_s t}, \quad \Delta \mathcal{M}_k(t) = A_M e^{-\alpha_m t}, \quad (4)$$

where $\alpha_{s,m}$ are system-size independent constants, $A_{s,m} \propto N$. The relevant long-time saturation values of PE (\mathcal{S}_2^∞) and SE (\mathcal{M}_2^∞) are equal to the values for Haar-random states, which, for $k = 2$, read $\mathcal{S}_2^{\text{Haar}} = \log_2[D+1] - 1$ and $\mathcal{M}_2^{\text{Haar}} = \log_2[D+3] - 2$ [45, 63]. Eq. (4) implies that $\Delta \mathcal{S}_k(t) \leq \epsilon$ for $t > t_{\text{sat}}^{(\mathcal{S}_k)} \propto \log_2(N)$, showing that the anticoncentration, $p_{\text{col}} \leq a^{-1}2^{-N}$, occurs on logarithmic timescales [3, 45]. Similarly, magic spreading follows an analogous behavior, with $\Delta \mathcal{M}_k(t) \leq \epsilon$ for $t > t_{\text{sat}}^{(\mathcal{M}_k)} \propto \log_2(N)$ [48]. The results of random quantum circuits will serve as a reference point in our investigation of the time evolution of PE and SE under dynamics of ergodic quantum many-body systems [5].

We consider two paradigmatic ergodic quantum many-body systems: a Kicked Ising model (KIM) [73–75], with Floquet operator defined by

$$U_{\text{KIM}} = e^{-ib \sum_j X_j} e^{-i \sum_j h_j Z_j + J \sum_j Z_j Z_{j+1}}. \quad (5)$$

and a mixed fields Ising model (MFIM) [76] with Hamiltonian given by

$$H_{\text{MFIM}} = b \sum_j X_j + \sum_j h_j Z_j + J \sum_j Z_j Z_{j+1}, \quad (6)$$

where b, h_j, J are parameters, which we fix as $b = (\sqrt{5} + 5)/8$, $h_i = (\sqrt{5} + 1)/4$, $J = 1$, following the choice of [76], and assume open boundary conditions for both models. The trends and conclusions of the following numerical investigations are expected to not depend on the precise choice of the parameters b, h_j, J , as long as the parameters are not fine-tuned to special cases in which the dynamics of the considered models simplifies, e.g., due to dual-unitarity of KIM (when $|b| = |J| = \pi/4$ [77–82]) or free-fermionicity of MFIM (when $h_j = 0$) [83]. We consider dynamics starting from the state of the form

$$|\Psi_0\rangle = \prod_{j=1}^N U_j^{(1)} |0\rangle^{\otimes N}, \quad (7)$$

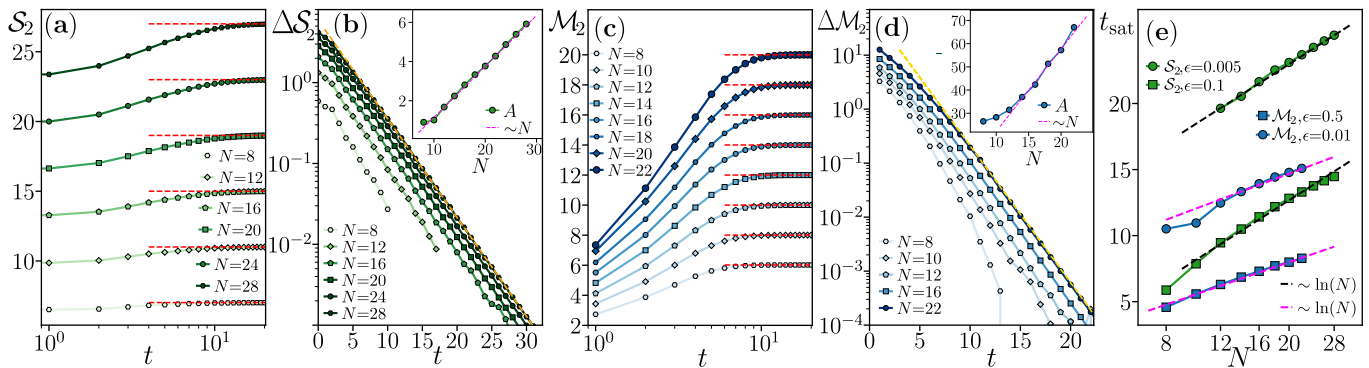


Figure 2. Anticoncentration and magic spreading in KIM for N qubits. (a) PE, $\mathcal{S}_2^{(2)}$, saturates to $\mathcal{S}_2^{\text{Haar}}$ (dashed line). (b) An exponential decay of $\Delta\mathcal{S}_2 = Ae^{-\alpha_S t}$ with time t , where $\alpha_S = 0.28(2)$, and $A \propto N$, see the inset. (c) the SE, \mathcal{M}_2 , abruptly saturates to $\mathcal{M}_2^{\text{Haar}}$ (dashed line). (d) The difference $\Delta\mathcal{M}_2$ is well fitted by an exponential decay, $\Delta\mathcal{M}_2 = Ae^{-\alpha_M t}$, with $\alpha_M = 0.59(3)$, and $A \propto N$, see the inset. (e) $\Delta\mathcal{S}_2$ and $\Delta\mathcal{M}_2$ decay to a given $\epsilon \lesssim O(1)$ at times $t_{\text{sat}} \propto \log_2(N)$ scaling logarithmically with system size N . The results are averaged over more than 200 initial states $|\Psi_0\rangle$ (7).

where $U_j^{(1)}$ are independent Haar-random unitaries acting on site j . We numerically calculate time-evolved state $|\Psi_t\rangle = U_{\text{KIM}}^t |\Psi_0\rangle$ for KIM employing fast Hadamard transform [84, 85], and $|\Psi_t\rangle = e^{-iH_{\text{MFIM}}t} |\Psi_0\rangle$ using Chebyshev time-evolution [86, 87]. In both cases, we compute the exact numerical representation $|\Psi_t\rangle = \sum_{\mathbf{x} \in \mathcal{B}} \langle \mathbf{x} | \Psi_t \rangle |\mathbf{x}\rangle$, calculate PE directly from the definition (1) and employ the algorithm of [88] to calculate SE. To obtain insights into the generic behavior of PE and SE in the dynamics of many-body systems, we average $\mathcal{S}_2(t)$ and $\mathcal{M}_2(t)$ over more than 200 choices of the initial states $|\Psi_0\rangle$.

Results for Floquet dynamics. We first study the anticoncentration and magic spreading in the Floquet dynamics of KIM, Eq. (5).

Our results are summarized in Fig. 2. First, we studied the anticoncentration of the time-evolved state. In the dynamics under U_{KIM} , energy is *not* conserved, and there are no other conserved quantities. Consequently, similarly to the case of random quantum circuits, we observe that PE and SE saturate for $t \gg 1$ to the values characteristic to Haar-random states up to corrections suppressed exponentially in N . In other words, we find that $\mathcal{S}_k^\infty = \mathcal{S}_k^{\text{Haar}}$, and $\mathcal{M}_k^\infty = \mathcal{M}_k^{\text{Haar}}$, as shown in Fig. 2 (a) and (c). Moreover, as shown in Fig. 2 (b), for $t \gtrsim 5$, the difference $\Delta\mathcal{S}_2(t) = \mathcal{S}_2^{\text{Haar}} - \mathcal{S}_2(t)$ decays exponentially in time as $\Delta\mathcal{S}_2 = Ae^{-\alpha_S t}$, where $\alpha_S = 0.28(2)$ is, at sufficiently large system size, independent of N . The parameter A scales linearly with N for $N \gtrsim 12$, see the inset in Fig. 2 (b). The extended range of system sizes $N \leq 28$ accessible to our computations allows us to observe a logarithmic scaling, $\tau_{\text{sat}}^{(\mathcal{S}_2)} \propto \log_2(N)$, of the time beyond which $\Delta\mathcal{S}_k < \epsilon$, as presented in Fig. 2 (e). Hence, the phenomenology of the PE growth and its saturation under dynamics of KIM fully parallels the random circuit models behavior [45].

We now turn to the analysis of the growth of SE \mathcal{M}_2 (similar results hold for other Rényi indices k , and

are not presented here for presentation purposes). The method [88] of SE computation allowed us to obtain numerically exact results for $N \leq 22$. In Fig. 2 (c) we show the evolution of SE as a function of time t for different system sizes. We observe a transient regime in which \mathcal{M}_2 increases rapidly before saturating to the Haar value $\mathcal{M}_2^{\text{Haar}}$ (dashed lines). In Fig. 2 (d), we present the results for $\Delta\mathcal{M}_2$ for different system sizes N , observing that $\Delta\mathcal{M}_2$ decays exponentially as a function of time t , and the prefactor A is proportional to the system size N , see the inset in Fig. 2 (d). Moreover, in Fig. 2 (e), we show the saturation time $t_{\text{sat}}^{(\mathcal{M}_2)}$ of SE as a function of system size N , observing logarithmic scaling of $t_{\text{sat}}^{(\mathcal{M}_2)}$ with the system size N , analogously as for the local random quantum circuits [48].

Results for Hamiltonian dynamics. We turn our attention to non-integrable Hamiltonian dynamics, focusing on the MFIM. For the chosen parameters, $b = (\sqrt{5} + 5)/8$, $h_i = (\sqrt{5} + 1)/4$, $J = 1$ the model is quantum ergodic [76], and its level statistics follows the predictions of Gaussian Orthogonal Ensemble of random matrices [89, 90]. The dynamics generated by Eq. (6) conserves the energy. As a result, in order to compare Floquet and Hamiltonian dynamics on the same foot, we consider initial states $|\Psi_0\rangle$ of the form (7), with additional constraint that $|\langle \Psi_0 | H_{\text{MFIM}} | \Psi_0 \rangle - E_{\text{min}}| / (E_{\text{max}} - E_{\text{min}}) \leq 0.05$, ensuring that the initial state has energy close to the middle of the spectrum (here E_{max} and E_{min} are respectively the highest state and the ground state energies of H_{MFIM}).

Our numerical results for PE and SE growth under the dynamics of MFIM are summarized in Fig. 3. The PE, \mathcal{S}_2 , is shown as a function of time t in Fig. 3 (a). Already at time $t = 1$, \mathcal{S}_2 is proportional to the system size N . At longer times, the PE saturates to a stationary value \mathcal{S}_2^∞ that is close, but noticeably differs from the Haar value $\mathcal{S}_2^{\text{Haar}}$. This is the first difference between the dynamics of MFIM and the results for Floquet and random quantum

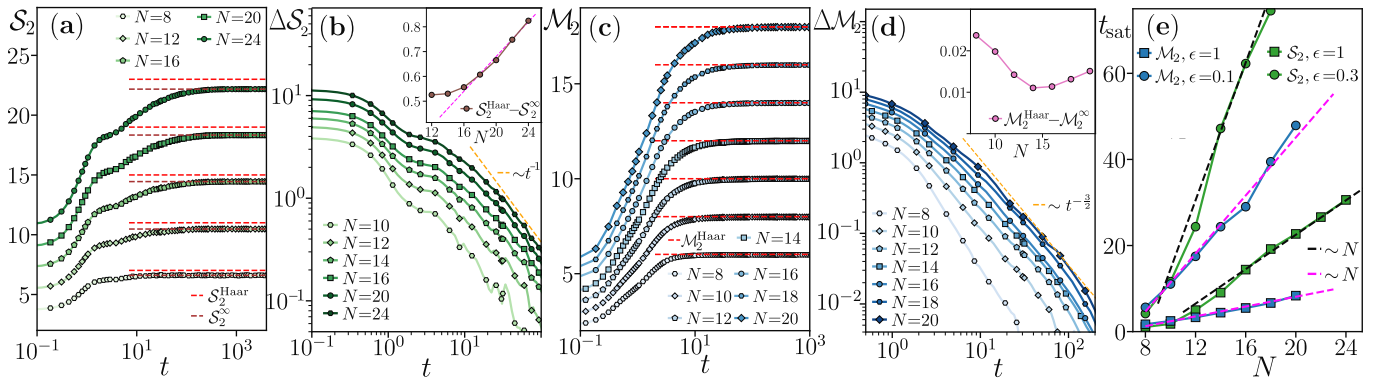


Figure 3. Anticoncentration and magic spreading in MFIM for N qubits. (a) The PE, $\mathcal{S}_2^{(2)}$, increases towards the long-time saturation value \mathcal{S}_2^∞ whose difference with $\mathcal{S}_2^{\text{Haar}}$ remains non-zero, see the inset in (b). The difference $\Delta\mathcal{S}_2$, see panel (b), follows a power-law decay, $\Delta\mathcal{S}_2 \propto t^{-\beta_S}$ with $\beta_S \approx 1$. (c) The SE, \mathcal{M}_2 , saturates to \mathcal{M}_2^∞ smaller than the Haar value $\mathcal{M}_2^{\text{Haar}}$, as shown in the inset in (d). The difference $\Delta\mathcal{M}_2$, shown in (d), is well fitted by a power-law decay $\Delta\mathcal{M}_2 \propto t^{-\beta_M}$ with $\beta_M \approx -1.5$. (e) $\Delta\mathcal{S}_2$ and $\Delta\mathcal{M}_2(t)$ decay to a given ϵ at times $t_{\text{sat}} \propto N$ scaling linearly with system size N .

circuit models. In Fig. 3 (b) we present the results for the difference $\Delta\mathcal{S}_2(t) = \mathcal{S}_2^\infty - \mathcal{S}_2(t)$ for various system sizes, where \mathcal{S}_2^∞ is computed by averaging $\mathcal{S}_2(t)$ over time interval $t \in [1000, 5000]$. For $t \gtrsim 5$, $\Delta\mathcal{S}_2$ decays as a power-law in time,

$$\Delta\mathcal{S}_2(t) = a_d t^{-\beta_S}, \quad (8)$$

where $\beta_S \approx 1.0$ (the accessible range of system sizes and time scales prevents us from pin-pointing the value of β_S). The algebraic decay (8) differs qualitatively from the exponential decay relevant for random quantum circuits (4). In the inset in Fig. 3 (b), we present the difference between the Haar value $\mathcal{S}_2^{\text{Haar}}$ and the long-time saturation value \mathcal{S}_2^∞ under the dynamics of MFIM. We observe that $\mathcal{S}_2^{\text{Haar}} - \mathcal{S}_2^\infty$ starts to increase linearly with system size for $N \geq 16$, which implies that $D_2 < 1$ in (2). Consequently, $p_{\text{col}} > 2^{-N}$ at sufficiently large N , meaning that the full anticoncentration of the time-evolved state $|\Psi_t\rangle$ in the computational basis \mathcal{B}_N is not observed, at least at the time scales and system sizes available to our numerical computations.

In Fig. 3 (c), we show the evolution of the SE for different sizes N . The initial state $|\Psi_0\rangle$ has a non-vanishing SE. Our data highlight a transient in which $\mathcal{M}_2(t)$ increases slower than the case of KIM, before saturating to the long-time value \mathcal{M}_2^∞ , which is close, but noticeably smaller than the Haar value $\mathcal{M}_2^{\text{Haar}}$, see the inset in Fig. 3 (d). For $t \gtrsim 1$, the difference $\Delta\mathcal{M}_2(t) = \mathcal{M}_2^\infty - \mathcal{M}_2(t)$ increases with the system size N and decays, see Fig. 3 (d) as a power-law in time:

$$\Delta\mathcal{M}_2(t) = a_d^\beta t^{-\beta_M}, \quad (9)$$

where a_d and $\beta_M \approx 1.5$ are constants. The power-law relaxation of the SE to their long-time saturation values under the dynamics of MFIM is one of the main results of this work. The power-law decay of $\Delta\mathcal{S}_2$ and $\Delta\mathcal{M}_2$ implies

that the saturation of PE and SE to their stationary values under dynamics of MFIM occurs at longer time scales than in KIM. In Fig. 3 (e) we show the the saturation time $t_{\text{sat}}^{(\mathcal{M}_2^{(2)})}$ as a function of N for different thresholds ϵ . The saturation times $t_{\text{sat}}^{(\mathcal{S}_2^{(2)})}$, $t_{\text{sat}}^{(\mathcal{M}_2^{(2)})}$ scale, with a good accuracy, linearly with the system size N , i.e. at times qualitatively longer than in the case of random quantum circuits and Floquet models. Finally, while the averaged $\mathcal{S}_2(t)$ and $\mathcal{M}_2(t)$ represent a typical time-evolution of PE and SE, we note that there is a non-negligible spread of $\mathcal{S}_2(t)$ and $\mathcal{M}_2(t)$ corresponding to the choice of the initial state $|\Psi_0\rangle$ for the dynamics of MFIM. This feature also distinguishes the Hamiltonian dynamics of MFIM from the Floquet models and random circuits, which we discuss in detail in the End Matter.

Discussion and conclusions. In this work, we studied the anticoncentration and magic resources growth in dynamics of ergodic quantum many-body systems. By using PE to characterize anticoncentration and SE to track the magic spreading, we examined the impact of energy conservation on these processes, comparing our findings with predictions from random circuit models.

Our numerical analysis reveals qualitatively distinct behaviors of Floquet and Hamiltonian systems. Floquet systems closely follow random circuit predictions, exhibiting analogous anticoncentration and magic spreading dynamics, with exponential relaxation of PE and SE towards the long-time saturation values with characteristic time scales logarithmically in system size N . In contrast, Hamiltonian systems demonstrate slower equilibration of both PE and SE. This discrepancy can be attributed to the energy conservation of the Hamiltonian dynamics, and the presence of atypical area-law entangled [91] low-lying eigenstates, which constrain the manifold of states explored by $|\Psi_t\rangle$ during its time-evolution, preventing PE and SE to reach values characteristic for

the typical Haar-random states $\mathcal{S}_2^{\text{Haar}}$ and $\mathcal{M}_2^{\text{Haar}}$.

Two striking consequences emerge from our findings. First, simulating anticoncentration and magic growth in many-body dynamics is computationally more efficient for quantum circuits than for Hamiltonian dynamics. Digital, e.g., Floquet systems saturate faster, allowing tensor network methods [92–94] to efficiently describe their evolution with polynomial bond dimensions. This has implications for approximate shadow tomography protocols that combine tensor networks with shallow circuits are significantly more efficient for digital systems than for Hamiltonian ones [95–100]. This also motivates further explorations of Clifford-augmented matrix product states [101–105] in scenarios where the dynamics are governed by continuous Hamiltonians.

Our findings open several avenues for future research. Energy conservation plays a major role in the anticoncentration and magic spreading. A systematic investigation of other conservation laws, such as continuous symmetries is essential. This may include analyzing the role of $U(1)$ or non-abelian symmetries and providing links between magic resources and the system’s slow hydrodynamic modes [106–109]. Furthermore, the impact of integrability [110] and ergodicity breaking [7, 8, 111], which provide additional constraints on the manifolds of states visited throughout the time evolution, on anticoncentration and magic spreading remains unresolved. These questions are left for future work.

Acknowledgements. We thank L. Leone, L. Piroli, T. Haug, M. Heinrich, for discussions, and J. De Nardis, G. Lami, G. Fux, P. Tarabunga, M. Frau, N. Dowling, P. Kos, M. Dalmonte, R. Fazio, M. Savage, C. Robin, P. R. Nicácio Falcão, P. Stornati, S. Masot-Llima, A. Garcia-Saez for collaborations on related topics. E. T. acknowledges support from ERC under grant agreement n.101053159 (RAVE), and CINECA (Consorzio Interuniversitario per il Calcolo Automatico) award, under the IS CRA initiative and Leonardo early access program, for the availability of high-performance computing resources and support. X.T. acknowledges support from DFG under Germany’s Excellence Strategy – Cluster of Excellence Matter and Light for Quantum Computing (ML4Q) EXC 2004/1 – 390534769, and DFG Collaborative Research Center (CRC) 183 Project No. 277101999 - project B01.

Data Availability. — Numerical data and snippets of the code are available in Ref. [112].

Note Added. — During the completion of this work, we become aware of a complementary study by the group of A. Hamma. This work will appear in the same arXiv posting [113]

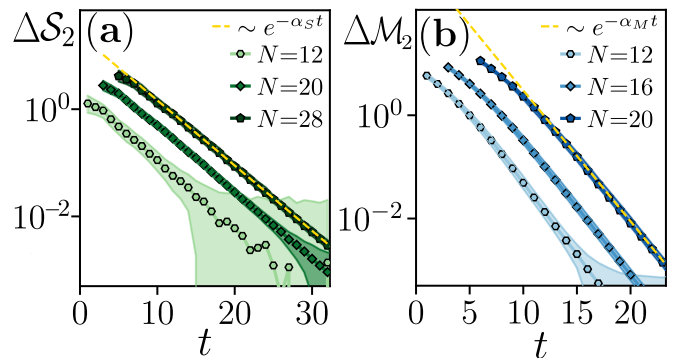


Figure 4. Initial state dependence of the saturation of PE, (a), and SE, (b), in KIM. The averaged ΔS_2 and ΔM_2 decrease exponentially in time t , and are well fitted by $e^{-\alpha S, M t}$, as discussed in the Main Text. The shaded regions represent the spread of ΔS_2 and ΔM_2 with the variation of the initial state $|\Psi_0\rangle$, (7). The lower/upper boundary of the shaded regions at fixed t correspond to 20th/80th percentile of the distribution of $\Delta S_2(t)$ and $\Delta M_2(t)$, respectively shown in (a) and (b). The data for $N = 20, 28$ in (a) and for $N = 16, 20$ in (b) have been shifted horizontally by factors of 4 and 8 for clarity of the plot.

End Matter.

In this work, we explored the dynamics of Hilbert space delocalization and magic spreading under unitary Hamiltonian evolution. Specifically, we examined two paradigmatic models of chaotic quantum dynamics: the Kicked Ising Model (KIM) and the Mixed Field Ising Model (MFIM). Our findings reveal striking differences in how these systems approach equilibrium, with the saturation behaviors of the participation entropy (PE) and stabilizer entropy (SE) serving as key indicators.

In the case of KIM, both PE and SE rapidly equilibrate to their long-time saturation values, which coincide with those of random Haar states. The saturation of PE and SE follows

$$\mathcal{S}_2 = \mathcal{S}_2^{\text{Haar}} - A e^{-\alpha s t} \quad \text{and} \quad \mathcal{M}_2 = \mathcal{M}_2^{\text{Haar}} - A e^{-\alpha M t} \quad (10)$$

In other words, Eqs.(10) imply that the PE and the SRE approach their stationary value, up to a fixed accuracy, at a time scaling logarithmically with the system size N .

In contrast, MFIM displays a qualitatively different behavior, with PE and SE approaching their saturation values according to power-law decay:

$$\mathcal{S}_2 = \mathcal{S}_2^\infty - a_d t^{-\beta_S} \quad \text{and} \quad \mathcal{M}_2 = \mathcal{M}_2^\infty - a_d^\beta t^{-\beta_M} \quad (11)$$

Here, the saturation values \mathcal{S}_2^∞ and \mathcal{M}_2^∞ deviate from the Haar state averages, and this discrepancy grows with increasing N . Additionally, the timescale for equilibration of PE and SE in MFIM scales linearly with N .

Here, we conduct an analysis of the PE and SE dynamics, focusing on their dependence on the choice of initial states. Figures 4 and 5 illustrate our findings.

In Fig. 4, we focus on the behavior PE and SE in KIM dynamics. Panels (a) and (b) depict the exponential decay of the average deviations of $\Delta\mathcal{S}_2$ and $\Delta\mathcal{M}_2$ from the long-time saturation values \mathcal{S}_2^∞ and \mathcal{M}_2^∞ across more than 200 randomly sampled initial states $|\Psi_0\rangle$ defined in Eq. 7. These deviations are well-fitted by $e^{-\alpha_S t}$ and $e^{-\alpha_M t}$ respectively. The shaded regions indicate the spread of $\Delta\mathcal{S}_2$ and $\Delta\mathcal{M}_2$ due to variation in the initial state, with the spread decreasing as the system size N increases. The decreasing spread shows that the saturation times $t_{\text{sat}}^{(\mathcal{S}_2)}$, $t_{\text{sat}}^{(\mathcal{M}_2)}$ discussed in the Main Text are well defined, and, for sufficiently large N , are independent of the choice of the initial state $|\Psi_0\rangle$.

In Fig. 5, we show analogous results for dynamics generated by the MFIM. Panels (a) and (b) demonstrate the power-law decay of the deviations $\Delta\mathcal{S}_2$ and $\Delta\mathcal{M}_2$, following t^{-1} and $t^{-3/2}$ respectively. The shaded regions represent the spread of these deviations across the initial states, which only slightly diminishes with increasing N . Consequently, the saturation times $t_{\text{sat}}^{(\mathcal{S}_2)}$, $t_{\text{sat}}^{(\mathcal{M}_2)}$ for *fixed initial state*, defined as times for which $\Delta\mathcal{S}_2(t) < \epsilon$ for a given initial state, are distributed over an interval which does not shrink with increasing N . The time scales $t_{\text{sat}}^{(\mathcal{S}_2)}$, $t_{\text{sat}}^{(\mathcal{M}_2)}$ presented in Fig. 3 (e) of the Main Text, obtained from the averaged $\Delta\mathcal{S}_2$ and $\Delta\mathcal{M}_2$, scale linearly with N , in the same way as analogous saturation times corresponding to *typical* $\Delta\mathcal{S}_2$ and $\Delta\mathcal{M}_2$ (data not shown). Panels (c) and (d) show the scaling of the saturation times with system size N , with shades corresponding to fixed lower and higher percentiles of the distribution of $\Delta\mathcal{S}_2(t)$ and $\Delta\mathcal{M}_2(t)$. While there is a significant spread of these time scales, we observe an increase of the saturation times corresponding to the fixed lower and higher percentiles, corroborating our conclusions about the PE and SE saturation under the dynamics of MFIM.

The results discussed here underscore the important role of the initial state in the dynamics of PE and SE, with this dependence being more pronounced in MFIM than in KIM. For the Floquet dynamics, the saturation of PE and SE, up to a fixed tolerance ϵ occurs at a well defined time scale, independent of the system size N (provided that N is large enough). In contrast, the specific choice of initial state can significantly affect the time scale at which PE and SE saturate under the dynamics of MFIM. In spite of this spread, the saturation times in the latter case are longer, with characteristic time scales increasing linearly with system size.

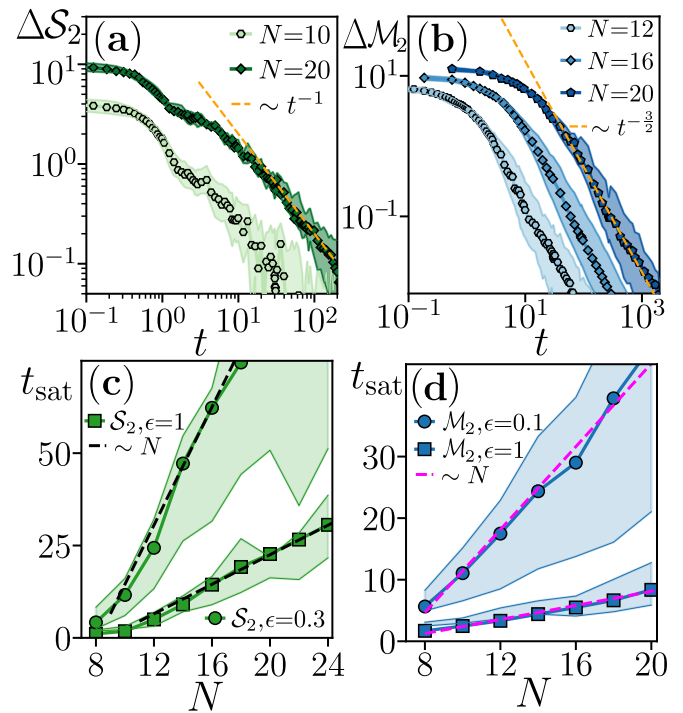


Figure 5. Initial state dependence of the saturation of PE, (a), and SE, (b), in MFIM. The shaded regions in (a) show the 33rd/66th percentile of the distribution of $\Delta\mathcal{M}_2(t)$, while, in (b), the shaded region boundaries correspond to 20th/80th percentile of the distribution of $\Delta\mathcal{S}_2(t)$. (c) and (d) show the saturation time scales $t_{\text{sat}}^{(\mathcal{S}_2, \mathcal{M}_2)}$ corresponding to the shaded regions of (a) and (b). The data for $N = 20$ in (a) and for $N = 16, 20$ in (b) have been shifted horizontally by multiplying by constant factors for clarity of the plot.

[1] R. Horodecki, P. Horodecki, M. Horodecki, and K. Horodecki, *Rev. Mod. Phys.* **81**, 865 (2009).
 [2] L. Amico, R. Fazio, A. Osterloh, and V. Vedral, *Rev. Mod. Phys.* **80**, 517 (2008).
 [3] A. M. Dalzell, N. Hunter-Jones, and F. G. S. L.

Brandão, *PRX Quantum* **3**, 010333 (2022).
 [4] Z.-W. Liu and A. Winter, *PRX Quantum* **3**, 020333 (2022).
 [5] L. D’Alessio, Y. Kafri, A. Polkovnikov, and M. Rigol, *Adv. Phys.* **65**, 239–362 (2016).
 [6] S. Pappalardi, L. Foini, and J. Kurchan, *Phys. Rev. Lett.* **129**, 170603 (2022).
 [7] D. A. Abanin, E. Altman, I. Bloch, and M. Serbyn, *Rev. Mod. Phys.* **91**, 021001 (2019).
 [8] P. Sierant, M. Lewenstein, A. Scardicchio, L. Vidmar, and J. Zakrzewski, *Rep. Prog. Phys.* (2024).
 [9] S. F. E. Oliviero, L. Leone, A. Hamma, and S. Lloyd, *npj Quantum Info.* **8**, 148 (2022).
 [10] P. Calabrese and J. Cardy, *J. Phys. A: Math. Theor.* **42**, 504005 (2009).
 [11] D. J. Luitz, F. Alet, and N. Laflorencie, *Phys. Rev. Lett.* **112**, 057203 (2014).
 [12] N. Macé, F. Alet, and N. Laflorencie, *Phys. Rev. Lett.* **123**, 180601 (2019).
 [13] P. Sierant and X. Turkeshi, *Phys. Rev. Lett.* **128**, 130605 (2022).
 [14] L. Leone, S. F. E. Oliviero, and A. Hamma, *Phys. Rev. Lett.* **128**, 050402 (2022).
 [15] L. Leone and L. Bittel, *Phys. Rev. A* **110**, L040403 (2024).
 [16] T. Haug and L. Piroli, *Phys. Rev. B* **107**, 035148 (2023).

- [17] M. P. Fisher, V. Khemani, A. Nahum, and S. Vijay, *Annu. Rev. Condens. Matter Phys.* **14**, 335 (2023).
- [18] A. Chan, A. De Luca, and J. T. Chalker, *Phys. Rev. X* **8**, 041019 (2018).
- [19] S. Shivam, A. De Luca, D. A. Huse, and A. Chan, *Phys. Rev. Lett.* **130**, 140403 (2023).
- [20] A. Nahum, S. Vijay, and J. Haah, *Phys. Rev. X* **8**, 021014 (2018).
- [21] L. Piroli, C. Sünderhauf, and X.-L. Qi, *J. High Energy Phys.* **2020** (4).
- [22] B. Bertini and L. Piroli, *Phys. Rev. B* **102**, 064305 (2020).
- [23] M. Fava, J. Kurchan, and S. Pappalardi, (2024), [arXiv:2308.06200](https://arxiv.org/abs/2308.06200) [quant-ph].
- [24] A. D. Luca, C. Liu, A. Nahum, and T. Zhou, [arXiv:2312.17744](https://arxiv.org/abs/2312.17744).
- [25] P. W. Claeys and A. Lamacraft, *Phys. Rev. Lett.* **126**, 100603 (2021).
- [26] S. Pappalardi, F. Fritzsche, and T. Prosen, (2024), [arXiv:2303.00713](https://arxiv.org/abs/2303.00713) [cond-mat.stat-mech].
- [27] N. Dowling, P. Kos, and K. Modi, *Phys. Rev. Lett.* **131**, 180403 (2023).
- [28] S. Boixo, S. V. Isakov, V. N. Smelyanskiy, R. Babbush, N. Ding, Z. Jiang, M. J. Bremner, J. M. Martinis, and H. Neven, *Nat. Phys.* **14**, 595 (2018).
- [29] F. Arute, K. Arya, R. Babbush, D. Bacon, J. C. Bardin, R. Barends, R. Biswas, S. Boixo, F. G. Brandao, D. A. Buell, *et al.*, *Nature* **574**, 505 (2019).
- [30] Y. Wu, W.-S. Bao, S. Cao, F. Chen, M.-C. Chen, X. Chen, T.-H. Chung, H. Deng, Y. Du, D. Fan, *et al.*, *Phys. Rev. Lett.* **127**, 180501 (2021).
- [31] A. Nahum, J. Ruhman, S. Vijay, and J. Haah, *Phys. Rev. X* **7**, 031016 (2017).
- [32] T. Zhou and A. Nahum, *Phys. Rev. B* **99**, 174205 (2019).
- [33] T. Zhou and A. Nahum, *Phys. Rev. X* **10**, 031066 (2020).
- [34] R. Vasseur, A. C. Potter, Y.-Z. You, and A. W. W. Ludwig, *Phys. Rev. B* **100**, 134203 (2019).
- [35] A. C. Potter and R. Vasseur, Entanglement dynamics in hybrid quantum circuits, in *Entanglement in Spin Chains* (Springer International Publishing, 2022) p. 211–249.
- [36] P. Sierant, M. Schirò, M. Lewenstein, and X. Turkeshi, *Phys. Rev. Lett.* **131**, 230403 (2023).
- [37] G. M. Sommers, S. Gopalakrishnan, M. J. Gullans, and D. A. Huse, *Phys. Rev. B* **110**, 064311 (2024).
- [38] D. Hangleiter and J. Eisert, *Rev. Mod. Phys.* **95**, 035001 (2023).
- [39] S. Bravyi and A. Kitaev, *Phys. Rev. A* **71**, 022316 (2005).
- [40] D. Gross, *J. Math. Phys.* **47**, 122107 (2006).
- [41] V. Veitch, S. A. H. Mousavian, D. Gottesman, and J. Emerson, *New J. Phys.* **16**, 013009 (2014).
- [42] D. Gottesman, in *Group 22 International Colloquium on Group Theoretical Methods in Physics*, edited by C. P. Williams (Berlin, Heidelberg, 1999) pp. 302–313.
- [43] D. Gottesman, *Chaos Solit. Fractals* **10**, 1749 (1999).
- [44] C. Bertoni, J. Haferkamp, M. Hinsche, M. Ioannou, J. Eisert, and H. Pashayan, *Phys. Rev. Lett.* **133**, 020602 (2024).
- [45] X. Turkeshi and P. Sierant, *Entropy* **26**, 471 (2024).
- [46] P. Braccia, P. Bermejo, L. Cincio, and M. Cerezo, *Quantum Mach. Intell.* **6**, 54 (2024).
- [47] D. García-Martín, P. Braccia, and M. Cerezo, (2024), [arXiv:2405.10264](https://arxiv.org/abs/2405.10264) [quant-ph].
- [48] X. Turkeshi, E. Tirrito, and P. Sierant, (2024), [arXiv:2407.03929](https://arxiv.org/abs/2407.03929) [quant-ph].
- [49] A. Christopoulos, A. Chan, and A. D. Luca, (2024), [arXiv:2404.10057](https://arxiv.org/abs/2404.10057) [cond-mat.stat-mech].
- [50] R. Moessner and S. L. Sondhi, *Nat. Phys.* **13**, 424–428 (2017).
- [51] A. Polkovnikov, K. Sengupta, A. Silva, and M. Venugaltore, *Rev. Mod. Phys.* **83**, 863 (2011).
- [52] C. E. Porter and R. G. Thomas, *Phys. Rev.* **104**, 483 (1956).
- [53] S. Mullane, *Sampling random quantum circuits: a pedestrian's guide* (2020), [arXiv:2007.07872](https://arxiv.org/abs/2007.07872) [quant-ph].
- [54] N. Laflorencie and S. Rachel, *J. Stat. Mech.: Theory Exp.* **2014**, P11013.
- [55] D. J. Luitz, X. Plat, N. Laflorencie, and F. Alet, *Phys. Rev. B* **90**, 125105 (2014).
- [56] D. J. Luitz, F. Alet, and N. Laflorencie, *Phys. Rev. B* **89**, 165106 (2014).
- [57] A. Bäcker, M. Haque, and I. M. Khaymovich, *Phys. Rev. E* **100**, 032117 (2019).
- [58] S. Aaronson and A. Arkhipov, in *Proceedings of the forty-third annual ACM symposium on Theory of computing* (2011) p. 333.
- [59] M. J. Bremner, A. Montanaro, and D. J. Shepherd, *Phys. Rev. Lett.* **117**, 080501 (2016).
- [60] A. Bouland, *Nat. Phys.* **15**, 159 (2019).
- [61] M. Oszmaniec, N. Dangniam, M. E. Morales, and Z. Zimborás, *PRX Quantum* **3**, 020328 (2022).
- [62] M. Beverland, E. Campbell, M. Howard, and V. Kliuchnikov, *Quantum Sci. Technol.* **5**, 035009 (2020).
- [63] X. Turkeshi, A. Dymarsky, and P. Sierant, [arXiv:2312.11631](https://arxiv.org/abs/2312.11631).
- [64] T. Haug and L. Piroli, *Quantum* **7**, 1092 (2023).
- [65] D. Gross, S. Nezami, and M. Walter, *Commun. Math. Phys.* **385**, 1325 (2021).
- [66] P. S. Tarabunga, E. Tirrito, M. C. Bañuls, and M. Dalmonte, *Phys. Rev. Lett.* **133**, 010601 (2024).
- [67] G. Lami and M. Collura, *Phys. Rev. Lett.* **131**, 180401 (2023).
- [68] P. S. Tarabunga, E. Tirrito, T. Chanda, and M. Dalmonte, *PRX Quantum* **4**, 040317 (2023).
- [69] E. Tirrito, P. S. Tarabunga, G. Lami, T. Chanda, L. Leone, S. F. E. Oliviero, M. Dalmonte, M. Collura, and A. Hamma, *Phys. Rev. A* **109**, L040401 (2024).
- [70] X. Turkeshi, M. Schirò, and P. Sierant, *Phys. Rev. A* **108**, 042408 (2023).
- [71] T. Haug, S. Lee, and M. S. Kim, *Phys. Rev. Lett.* **132**, 240602 (2024).
- [72] M. Collura, J. D. Nardis, V. Alba, and G. Lami, (2024), [arXiv:2412.05367](https://arxiv.org/abs/2412.05367) [quant-ph].
- [73] T. Prosen, *Phys. Rev. Lett.* **80**, 1808 (1998).
- [74] T. Prosen, *Phys. Rev. E* **60**, 3949 (1999).
- [75] T. Prosen, *Phys. Rev. E* **65**, 036208 (2002).
- [76] H. Kim and D. A. Huse, *Phys. Rev. Lett.* **111**, 127205 (2013).
- [77] M. Akila, D. Waltner, B. Gutkin, and T. Guhr, *J. Phys. A: Math. Theor.* **49**, 375101 (2016).
- [78] B. Bertini, P. Kos, and T. Prosen, *Phys. Rev. Lett.* **121**, 264101 (2018).
- [79] B. Bertini, P. Kos, and T. Prosen, *Phys. Rev. Lett.* **123**, 210601 (2019).
- [80] B. Bertini, K. Klobas, and T.-C. Lu, *Phys. Rev. Lett.*

- 129**, 140503 (2022).
- [81] M. A. Rampp, R. Moessner, and P. W. Claeys, *Phys. Rev. Lett.* **130**, 130402 (2023).
- [82] A. Foligno, P. Kos, and B. Bertini, *Phys. Rev. Lett.* **132**, 250402 (2024).
- [83] In the dual-unitary limit, the evolution of PE has been studied in Ref. [114] while that of ME in Ref. [115, 116]. The magic spreading under free fermionic Hamiltonian evolution has been studied in Ref. [117].
- [84] T. L. M. Lezama, S. Bera, and J. H. Bardarson, *Phys. Rev. B* **99**, 161106 (2019).
- [85] P. Sierant, M. Lewenstein, A. Scardicchio, and J. Zakrzewski, *Phys. Rev. B* **107**, 115132 (2023).
- [86] H. Tal-Ezer and R. Kosloff, *J. Chem. Phys.* **81**, 3967 (1984).
- [87] P. Sierant and J. Zakrzewski, *Phys. Rev. B* **105**, 224203 (2022).
- [88] P. Sierant *et al.*, To appear.
- [89] M. L. Mehta, *Random Matrices* (Elsevier, Amsterdam, 1990).
- [90] F. Haake, *Quantum Signatures of Chaos* (Springer, Berlin, 2010).
- [91] J. Eisert, M. Cramer, and M. B. Plenio, *Rev. Mod. Phys.* **82**, 277 (2010).
- [92] U. Schollwöck, *Ann. Phys.* **326**, 96 (2011).
- [93] R. Orús, *Nat. Rev. Phys.* **1**, 538–550 (2019).
- [94] S.-J. Ran, E. Tarrico, C. Peng, X. Chen, L. Tagliacozzo, G. Su, and M. Lewenstein, *Tensor network contractions: methods and applications to quantum many-body systems* (Springer Nature, 2020).
- [95] H.-Y. Huang, R. Kueng, and J. Preskill, *Nat. Phys.* **16**, 1050 (2020).
- [96] H.-Y. Huang, *Nat. Rev. Phys.* **4**, 81 (2022).
- [97] M. McGinley and M. Fava, *Phys. Rev. Lett.* **131**, 160601 (2023).
- [98] M. Heinrich, M. Kliesch, and I. Roth, (2023), [arXiv:2212.06181 \[quant-ph\]](https://arxiv.org/abs/2212.06181).
- [99] R. Brieger, M. Heinrich, I. Roth, and M. Kliesch, (2023), [arXiv:2310.19947 \[quant-ph\]](https://arxiv.org/abs/2310.19947).
- [100] G. E. Fux, B. Béri, R. Fazio, and E. Tarrico, (2024), [arXiv:2410.09001 \[quant-ph\]](https://arxiv.org/abs/2410.09001).
- [101] S. Masot-Llima and A. Garcia-Saez, *Phys. Rev. Lett.* **133**, 230601 (2024).
- [102] X. Qian, J. Huang, and M. Qin, *Phys. Rev. Lett.* **133**, 190402 (2024).
- [103] G. Lami, T. Haug, and J. D. Nardis, [arXiv:2404.18751](https://arxiv.org/abs/2404.18751).
- [104] X. Qian, J. Huang, and M. Qin, (2024), [arXiv:2407.03202 \[cond-mat.str-el\]](https://arxiv.org/abs/2407.03202).
- [105] A. C. Nakhil, B. Harper, M. West, N. Dowling, M. Sevior, T. Quella, and M. Usman, (2024), [arXiv:2411.12482 \[quant-ph\]](https://arxiv.org/abs/2411.12482).
- [106] V. Khemani, A. Vishwanath, and D. A. Huse, *Phys. Rev. X* **8**, 031057 (2018).
- [107] C. W. von Keyserlingk, T. Rakovszky, F. Pollmann, and S. L. Sondhi, *Phys. Rev. X* **8**, 021013 (2018).
- [108] T. Rakovszky, F. Pollmann, and C. W. von Keyserlingk, *Phys. Rev. Lett.* **122**, 250602 (2019).
- [109] A. A. Michailidis, D. A. Abanin, and L. V. Delacrétaz, *Phys. Rev. X* **14**, 031020 (2024).
- [110] L. Vidmar and M. Rigol, *J. Stat. Mech: Theory Exp.* **2016**, 064007 (2016).
- [111] M. Serbyn, D. A. Abanin, and Z. Papić, *Nature Physics* **17**, 675 (2021).
- [112] Data available at publication on zenodo.
- [113] A. Hamma *et al.*, To appear.
- [114] P. W. Claeys and G. D. Tomasi, (2024), [arXiv:2408.02732 \[quant-ph\]](https://arxiv.org/abs/2408.02732).
- [115] J. A. Montaña López and P. Kos, *J. Phys. A: Math. and Theor.* **57**, 475301 (2024).
- [116] N. Dowling, P. Kos, and X. Turkeshi, (2024), [arXiv:2408.16047 \[quant-ph\]](https://arxiv.org/abs/2408.16047).
- [117] D. Rattacaso, L. Leone, S. F. E. Oliviero, and A. Hamma, *Phys. Rev. A* **108**, 042407 (2023).